DKH-DFT calculations of the structures, energies, and electrical and magnetic properties of Fe_n ($2 \leqslant n \leqslant 13$) clusters

Lucas S. C. Martins[1], Carolayne S. Gomes[2], Francisco E. Jorge[2,3*]

[1]Instituto Federal de Educação, Ciência e Tecnologia do Espírito Santo - Campus Linhares, 29901-291 Linhares, ES, Brazil

[2]Departamento de Física, Universidade Federal do Espírito Santo, 29060-900 Vitória, ES, Brazil

[3]Departamento de Física, Instituto de Ciências Exatas e Biológicas, Universidade Federal de Ouro Preto, Campus Universitário Morro do Cruzeiro, 35402-136 Ouro Preto, MG, Brazil

[*]E-mail: francisco.jorge@ufes.br

Abstract

At the DKH2-B1B95/DZP+1*d*-DKH level of theory, the following quantities were calculated: bond lengths, binding energies, equilibrium dissociation energies, HOMO-LUMO energy gaps, vertical ionization potentials, second-order differences in total energies, and spin magnetic moments of small iron clusters. The findings of this study closely align with the experimental values reported in the extant literature. The spin magnetic moments of the iron cluster cations examined in this study are among the most precise values reported to date. This finding lends credibility to the predicted geometric structures of the ground state and will undoubtedly facilitate the elucidation of the long-standing controversy surrounding the electronic structures of small iron clusters. The geometric structure for Fe_7 and the symmetries for Fe_5, Fe_6, Fe_8, Fe_9, and Fe_{12} found in this work for the ground state differ from those previously reported. The findings of this study indicate that Fe_5 and Fe_6 are the most stable clusters, while Fe_9 and Fe_{12} are the most reactive. In order to enhance comprehension of iron cluster electronic structures, we have computed static mean dipole polarizabilities and polarizability anisotropies for the first time.

Keywords: Relativistic calculations; iron clusters; structures; energies; electrical and magnetic properties

PACS: 31.15.aj, 31.15.E-, 36.40.Cg, 36.40.Mr

1. Introduction

The formation of clusters, whether composed of a small number of atoms or a substantial quantity, signifies an intermediate state between the microscopic and macroscopic realms. This is attributed to the significant disparities in the equilibrium electronic structures of clusters when compared to those of bulk materials.[1] Consequently, it can be deduced that clusters represent a distinct phase of matter, characterized by their inherent and distinctive properties. Transition metal clusters have been the focus of extensive research, employing a range of theoretical methods and experimental techniques. The determination of their electrical, magnetic, and structural properties can lead to significant advancements in various areas of nanotechnology. A series of investigations have confirmed that the magnetic moments of cobalt, iron, and nickel clusters[2-5] are greater than those of the respective bulk materials.[3] For cobalt and nickel clusters, a rapid convergence to the bulk value was observed,[6] whereas for iron clusters, a slow convergence was detected. Even clusters containing hundreds of iron atoms exhibited magnetization above the bulk value.[6] Additionally, several magnetization peaks were observed for this material. Iron clusters are of particular interest due to the substantial variation in their magnetic,[6–8] electronic,[9,10] reactivity,[11,12] and catalytic[13] properties with increasing numbers of atoms. These properties present challenges for theorists and experimentalists alike. Additionally, these materials find application in the fabrication of magnetic storage devices.

A variety of experimental techniques were employed to investigate the properties of iron clusters. These techniques included photoionization studies,[10,14] chemical probes,[15,16] time-of-flight (TOF) mass spectrometry,[17] collision-induced dissociation experiments,[9] photoelectron spectroscopy,[18] Stern–Gerlach measurements,[7,8] and X-ray magnetic circular dichroism spectroscopy.[19,20] The results

of these studies indicated a dependence of the magnitude of a property on the change in geometric structure as cluster size increases. Stern–Gerlach experiments are utilized to ascertain the total magnetic moments of gas-phase transition metal clusters. The experiments have measured magnetic moments ranging from 2.5 to 5.4 μB per atom for small iron clusters.[6-8,21,22] This is considerably larger than the bulk value of 2.2 μB.[19] Spin and orbital magnetic moments for cationic iron clusters were measured using circular magnetic X-ray dichroism spectroscopy.[19,20] The results indicate that spin magnetic moments are larger than orbital magnetic moments by a factor ranging from 2.5 to 20. As the number of atoms in a cluster decreases, its properties become size-dependent. In this context, determining the ground-state structure of the cluster is of paramount importance. A number of experimental techniques have been developed to provide information about cluster structure. These techniques include mobility measurements, Raman spectroscopy, and chemisorption on cluster surfaces. Despite the strides made in these techniques over the past few decades, they frequently fail to offer definitive evidence regarding the geometry of a particular cluster.

From a theoretical perspective, difficulties in addressing small transition metal clusters arise from the diverse possible structures and multiplicities resulting from an incomplete *d*-shell. Consequently, accurate *ab initio* or semi-empirical calculations of transition metal clusters pose significant challenges.[23] An alternative approach involves the utilization of density functional theory (DFT) to ascertain the various isomers of each cluster. This method incorporates electronic correlation and requires a computational time that is less than that of any post-Hartree-Fock method. Additionally, the DFT has been demonstrated to exhibit enhanced precision in comparison to semi-empirical methodologies. However, determining the lowest energy structure of a

moderately sized cluster with DFT is not computationally straightforward, since the number of atomic configurations to be tested increases with the size of the cluster.

DFT has been employed to predict the geometric and electronic structures of Fe_n clusters. However, the majority of these calculations have been conducted on clusters with $n \leq 7$. Chen *et al*.,[24] Castro and Salahub,[25] Ballone and Jones,[26] and Oda *et al*.[27] employed DFT to examine the properties of Fe_n clusters with $n \leq 4$, $n \leq 5$, $n \leq 7$, and $n \leq 5$, respectively. Calculations for $n > 7$ were performed using less accurate methods, such as the tight-binding method with adjustable parameters.[28] The limited size of the iron clusters studied up to 2000 prevented comparisons between experimental and theoretical data. A more profound comprehension of the properties of these clusters is of interest to fundamental physics, as well as to the nanotechnology and recording industries.[29] In 2001, Diéguez *et al*.[30] conducted calculations for iron clusters containing up to 17 atoms, employing the local spin density approximation (LSDA) for exchange and correlation, nonlocal pseudopotentials, and a basis set formed from a linear combination of numerical atomic orbitals (LCNAO). Köhler *et al*.[31] investigated the structural and magnetic properties of clusters containing up to 32 iron atoms. The researchers employed a methodology known as density functional based tight-binding (DFTB), which is an approximation of DFT, together with a linear combination of Slater-type orbitals (LCSTO). The BLYP functional with the double numerical basis set plus polarization functions (DNP) was utilized to ascertain the structures, binding energies, and magnetic moments of Fe_n clusters (n = 2–13, 15, and 19).[32] Concurrently, the OPBE functional was employed in conjunction with a triple zeta valence (TZV) quality basis set to determine the structures and energies of Fe_n clusters (n = 2–10).[33] Aktürka and Sebetci[34] presented a study of some properties of Fe_n clusters (n = 2–20). Initially, the DFTB approximation in conjunction with basin hopping was employed to ascertain

the lowest energy isomers of the clusters. Subsequently, the energies, magnetic moments, and harmonic vibrational frequencies were calculated using DFT. The BLYP functional and two basis sets were employed in the DFT calculations: the first was the relativistic SDD set with an effective core potential (ECP), and the second was the 6-31G** basis set for all electrons. A rapid review of the results obtained through these methodologies reveals inconsistencies in determining the geometric structure of the lowest-energy isomer of a given cluster and in the magnitudes of the computed properties. While semi-empirical potentials and parameter adjustment methods require less time to perform property calculations than DFT, the results obtained with these approximations are generally less accurate and reliable. Within the DFT framework, exchange and correlation energies are adjusted using a functional. A plethora of functionals have been documented in the extant literature, which can be categorized into five distinct classifications.[35] Hybrid functionals are the most prevalent and are among the most precise. It is imperative to emphasize that the outcomes of the calculated cluster properties are contingent on the basis set employed.

The iron atom possesses a total of 26 electrons and a ground state electronic configuration of [Ar]3$d^6$4s^2. It is noteworthy that four of these electrons are unpaired. This number of simply occupied atomic orbitals indicates that the possible multiplicities of any iron cluster containing multiple atoms can be substantial, with some potentially reaching extremely high values. In contrast to the majority of previous studies, we conducted a comprehensive evaluation, testing a minimum of ten multiplicities for each Fe_n and Fe_n^+ cluster. Given iron's position as a third-row element in the periodic table, the electron correlation and scalar relativistic correction must be taken into account in the calculation of iron clusters. This represents a significant challenge for any theoretical model. In addition to the absence of consensus regarding the geometric

structure of the ground state of a given iron cluster, the determination of the spin magnetic moment constitutes another point of contention among the various theoretical procedures utilized. A number of articles on iron clusters have been published in the literature.[30,31] These articles employed either LSDA or DFTB. The former is known to produce inaccurate results for binding energies and spin magnetic moments, while the latter, being an approximation of DFT, is also imprecise. With the exception of the BLYP/SDD calculations performed by Aktürka and Sebetci,[34] none of the other studies make use of any relativistic correction to analyze iron clusters. Section 3 will demonstrate that this can affect the results of properties involving the clusters' total energies.

In this study, we present a novel approach to investigating Fe_n clusters ($n \leq 13$) that combines the scalar relativistic Douglas-Kroll-Hess (DKH) approximation[36,37] with relativistic basis sets for all electrons. This theoretical model has previously been utilized in the study of transition metal clusters.[38-43] The primary advantage of this method is that the total energies calculated using this approach are generally more reliable than those obtained using effective core potentials, pseudopotentials, and non-relativistic procedures. Given the utilization of basis sets for all electrons, our approach will entail the application of our accumulated experience and literature data to minimize the number of isomers to be examined for each cluster.

The primary objective of this article is to facilitate comprehension of the discordant points reported in the extant literature concerning iron clusters. In order to achieve this objective, it was necessary to determine several key parameters. These included bond lengths (r_e), binding energies (*BE*), HOMO-LUMO energy gaps (E_g), equilibrium dissociation energies (D_e), vertical ionisation potentials (*VIP*), second-order differences in total energies ($\Delta^2 E$), and total spin magnetic moments (μ_T). A comparison

was made with available experimental data and the most recent theoretical results published in the literature. The results of the static mean dipole polarizabilities ($\overline{\alpha}$) and polarizability anisotropies ($\Delta\alpha$) facilitate comprehension of the reactivity and stability of the clusters. To the best of our knowledge, these two properties had not been previously considered in any studies of iron clusters.

2. Computational details

The scalar relativistic effect was considered in the calculations in this study because iron is a third-row element of the periodic table. To this end, the second-order DKH Hamiltonian (DKH2), as implemented in the Gaussian 09 code[44] with the all-electron DKH basis set of double zeta valence quality plus polarization functions (DZP-DKH),[45] was employed. As the *d* orbitals play a pivotal role in the description of the chemical bonds of iron clusters, a diffuse Gaussian function was incorporated into the original basis set. This function was obtained during the generation of the augmented non-relativistic basis set ADZP.[46] This modified set is henceforth referred to as DZP+1*d*-DKH. In order to obtain accurate results regarding polarizability, it is necessary to employ an augmented basis set containing diffuse functions[46] for the purpose of adequately describing the electrons that are most distant from the atomic nuclei. Consequently, a diffuse function was incorporated for each atomic symmetry (*s*, *p*, *d*, and *f*) into the DZP-DKH set.[45] These functions were again taken from the ADZP set.[46] Henceforth, this set will be referred to as the ADZP-DKH. The efficacy of these basis sets in determining the properties of transition metal clusters is evident in the Refs. [38,40,43]. Subsequent to the selection of the basis set, it is imperative to investigate which functional, when combined with this set, best describes the iron clusters. For this purpose, Fe_2 was initially selected as it is the smallest cluster studied and has several available experimental values in the literature. Table 1 presents the functionals that were

examined in conjunction with the DZP+1*d*-DKH basis set. All theoretical procedures predicted a multiplicity (M) of 7 and a bond length between 1.96 and 2.08 Å for the iron dimer. These values are in good agreement with the experimental measurements of (1.87±0.13)[47] and (2.02±0.02)[48] Å obtained in argon and neon matrices, respectively. With the exception of the B1B95 and BMK functionals, which have binding energies of 1.15 and 0.34 eV, respectively, that are in excellent and poor agreement with the experimental value of (1.14±0.10) eV,[9] the other functionals overestimate this latter value. Even when the zero-point vibrational correction of -0.05 eV is added to the B1B95 binding energy of 1.15 eV, the result remains within the experimental uncertainty bars. One reason why the experimental fundamental vibrational frequency[49] is overestimated by all theoretical frequencies is that the anharmonic vibrational correction was not considered in the latter's calculations. The magnitude of these errors is mitigated by the multiplication of harmonic vibrational frequencies by a scale factor that is less than one (see, for example, Ref. [50]). Another source of error was attributed to the intrinsic inability of LSDA and GGA functionals to determine the harmonic vibrational frequencies of iron clusters.[25] With regard to ionization potentials, some functionals overestimate and others underestimate the experimental value of (6.30±0.01) eV.[51] The most optimal result, 6.34 eV, was obtained using the B3LYP functional. The calculated spin magnetic moment (μ_T) of B1B95 is 6.0 μ_B, which is precisely midway between the experimentally predicted range of (6.5±1) μ_B.[7] Overall, the hybrid meta-GGA functional B1B95 demonstrated the optimal performance. In addition, given its recent successful application by our research group in the study of cobalt clusters,[43] as well as by other authors,[52] it was selected for further investigation. In summary, our experience has demonstrated that the DKH2-B1B95/DZP+1*d*-DKH theoretical

procedure can serve as a powerful and advantageous instrument for the investigation of transition metal clusters.

Table 1. Bond lengths (r_e), binding energies (*BE*), harmonic vibrational frequencies (ω_e), and vertical ionization potentials (*VIP*) of ground-state[a] Fe_2 calculated with the DZP+1*d*-DKH basis set and different functionals.

Method	r_e (Å)	*BE* (eV)	ω_e (cm^{-1})	*VIP* (eV)
DKH2-BLYP	2.01	2.06	409.4	6.56
DKH2-B3LYP	1.98	1.64	451.3	6.34
DKH2-BB95	2.00	2.57	416.6	6.65
DKH2-BPBE	2.00	2.10	419.2	6.60
DKH2-PBEPBE	2.00	2.30	417.6	6.57
DKH2-SVWN5	1.96	3.59	449.2	7.00
DKH2-TPSSh	1.98	0.90	446.3	6.19
DKH2-BP86	2.00	2.24	422.1	6.80
DKH2-B1B95	1.96	1.15	467.3	6.04
DKH2-APFD	2.08	1.78	624.8	5.68
DKH2-mPWPW91	2.00	2.20	418.8	6.64
DKH2-G96PW91	2.00	2.95	422.3	6.51
DKH2-BMK	1.96	0.34	511.3	5.89
Experimental	(1.87±0.13)[b] (2.02±0.02)[c]	(1.14±0.10)[d]	299.6[e]	(6.30±0.01)[f]

[a]Multiplicity equal to 7. [b]From Ref. [47]. [c]From Ref. [48]. [d]From Ref. [9]. [e]From Ref. [49]. [f]From Ref. [51].

For the purpose of comparison, a selection of results for Fe_2 was obtained through the utilization of disparate theoretical models. The bond lengths obtained in Refs. [33,34] demonstrate strong agreement with the experimental value of (2.02 ± 0.02)[48] Å and approximate proximity to the B1B95/DZP+1d-DKH value. However, it is notable

	r_e (Å)	*BE* (eV)	ω_e (cm^{-1})	μ_T (μ_B)
BLYP/SDD-ECP[34]	2.02	1.51	393.0	6
BLYP/6-31G**[34]	2.03	1.69	416.1	8

OPBE/TZV[33]	2.00	1.24	397.9	6

that the binding energies and harmonic vibrational frequencies[33,34] are found to be overestimated. With the exception of the spin magnetic moment, which was determined using the BLYP/6-31G** theory level, the remaining values correspond to the values predicted by the present study. The relativistic BLYP/SDD-ECP results demonstrate a higher degree of correlation with the experimental data compared to the non-relativistic BLYP/6-31G** results. It is important to note that the SDD basis set exclusively describes valence electrons, whereas the 6-31G** set encompasses all electrons.

The following equations were utilized to compute the properties of Fe_n ($2 \leq n \leq 13$):

$$BE = n\,E(\mathrm{Fe}) - E(\mathrm{Fe_n}), \quad (1)$$

$$D_e = E(\mathrm{Fe_{n-1}}) + E(\mathrm{Fe}) - E(\mathrm{Fe_n}), \quad (2)$$

$$\Delta^2 E = E(\mathrm{Fe_{n+1}}) + E(\mathrm{Fe_{n-1}}) - 2\,E(\mathrm{Fe_n}), \quad (3)$$

$$VIP = E(\mathrm{N}-1) - E(\mathrm{N}), \quad (4)$$

$$E_g = E(\mathrm{LUMO}) - E(\mathrm{HOMO}), \quad (6)$$

$$\bar{\alpha} = (\alpha_{xx} + \alpha_{yy} + \alpha_{zz})/3\,, \quad (7)$$

$$\Delta\alpha = \sqrt{1/2}[(\alpha_{xx} - \alpha_{yy})^2 + (\alpha_{yy} - \alpha_{zz})^2 + (\alpha_{zz} - \alpha_{xx})^2 + 6\alpha_{xy}^2]^{1/2}, \quad (8)$$

where E, N and n represent the total energy, number of electrons, and number of atoms in a cluster, respectively, and α_{xx}, α_{xy}, etc. represent the components of the polarizability tensor.

A comprehensive investigation was initially conducted to ascertain the geometric structures and the multiplicities of the ground state of the iron clusters. Subsequently, the electronic, electrical, and magnetic properties were calculated from these structures.

3. Results and discussion

3.1. Finding the most stable geometric structures

As previously stated, this work utilizes the relativistic DZP+1*d*-DKH basis set to describe all electrons in each iron cluster. Consequently, as the number of atoms in the cluster increases, the calculation becomes more computationally expensive. In order to reduce the time required for the execution of this arduous task, the accumulated experience of the our research group was utilized, with the process beginning with the geometric structures of iron clusters that have been reported in the existing literature[24-34] and continuing with the structures that had previously been determined in the our research group's work on cobalt, copper, rhodium, silver, iridium, and gold clusters.[38-43] For each geometric structure of an iron cluster that was used as a starting point, different multiplicities were tested in order to find the one with the lowest energy. It is important to note that no restrictions were imposed during the geometry optimization process.

The initial geometric structures employed for the iron trimer were linear and isosceles and equilateral triangles. For each of these, multiplicities of 9, 11, and 13 were tested. Subsequent to optimization at the DKH2-B1B95/DZP+1*d*-DKH theoretical level, the three equilateral triangles were reduced to isosceles triangles. The geometric structure that exhibited the lowest energy was the isosceles triangle, with M = 13. This structure exhibits a marginal increase in stability, with a value of 0.28 kcal/mol, in comparison to the linear structure with M = 11 (refer to Figure 1). In accordance with theoretical predictions, alternative approaches[32,33,53] predicted an isosceles triangle as the lowest-energy structure of Fe_3. However, Diéguez *et al.*[30] and Aktürk and Sebetci[34] reported equilateral and scalene triangles, respectively. In 1985, Micklitz *et al.*[54] arrived at the conclusion that Fe_3 possesses a triangular structure, a conclusion that was derived from experimental measurements.

The ground state of the iron tetramer has been the subject of investigation in a variety of geometric forms, including tetrahedral, rectangular, rhomboid, and square geometries.[24,25,30-34,53] The majority of these studies suggest that the structure of the lowest-energy isomer of this cluster is a regular[24,25] or distorted[30,32-34] tetrahedron. In the context of the cobalt tetramer, it was observed that the tetrahedral and rhomboid structures exhibited a high degree of similarity in their total energies.[43] Consequently, a decision was made to undertake a re-examination of these geometries, in addition to multiplicities 9, 11, 13, and 15, within the scope of the present study. The DKH2-B1B95/DZP+1*d*-DKH theoretical model, which is initiated with a structure exhibiting T_d symmetry, predicts a distorted tetrahedral structure with D_{2d} symmetry and M = 15 for the ground state of Fe_4. The total energy of a similar structure with M = 13 differs by only 0.26 kcal/mol from the previous one. The most stable rhombic structure predicted by the model has a multiplicity of 15, with a total energy 4.64 kcal/mol above that of the ground state (see Fig. 1). The predictions by Diéguez *et al.*[30] and Cervantes-Salguero and Seminario[33] indicate that the lowest-energy structure of Fe_4 belongs to the D_{2d} point group, a finding that aligns with the present study's conclusions.

The extant literature on the subject, specifically referenced in the text as [30-34], agrees that the lowest energy structure for Fe_5 is a trigonal bipyramid. However, a consensus has yet to be reached regarding its point group classification. At the BLYP/SDD and BLYP/6-31G** levels of theory, Aktürk and Sebetci[34] identified C_{2v} and C_s symmetries, respectively. In a separate study, Ma *et al.*[32] employed the BLYP/DNP theoretical model to identify D_{3h}. As with cobalt clusters,[43] W-like, trigonal bipyramidal, and square pyramidal geometric structures were investigated. For each structure, multiplicities of 15, 17, and 19 were tested. Following the optimization process, the initial symmetries D_{3h} and C_{4v} underwent a relaxation to C_1, while C_{2v} was

sustained. The DKH2-B1B95/DZP+1*d*-DKH calculations for Fe_5 yielded two lowest-energy structures: distorted trigonal bipyramids with multiplicities of 19 and 17, respectively. The latter exhibited an energy of 10.16 kcal/mol higher. To the best of our knowledge, this is the first report of a geometric structure with C_1 symmetry for the ground state of the pentamer.

A substantial amount of research in the literature supports the hypothesis that a regular octahedron (O_h symmetry)[31] and a distorted octahedron (D_{4h} symmetry)[30,32,33,34] could serve as the hexamer ground state. For the present study, three structures were selected as the starting points: a boat shape, a pentagonal pyramid, and an octahedron with C_s, C_{5v}, and O_h symmetries, respectively. For each structure, the multiplicities of 19, 21, and 23 were examined. Subsequent to optimization, structures exhibiting C_{5v} symmetry underwent a transformation, acquiring a distorted octahedral configuration with C_1 symmetry. The remaining structures exhibited C_s and O_h symmetries, as illustrated in Fig. 1. The lowest-energy structure was determined to be an octahedron belonging to the C_1 point group with M = 21. The second lowest energy structure was boat-shaped with C_s symmetry and M = 21, with a total energy of 4.15 kcal/mol above the ground state.

A regular pentagonal bipyramid (D_{5h})[30-32] or distorted pentagonal bipyramid (C_1 and C_s)[33,34] has been reported as the heptamer's lowest energy structure. We considered multiplicities of 19, 21, and 23 for a capped octahedron (C_{3v}) and a pentagonal bipyramid (D_{5h}). It has been demonstrated that, given the absence of any restrictions imposed on the optimization process, the symmetries of the two lowest-energy structures are reduced to C_1 and C_{2v}, respectively, with M = 23 (Fig. 1). The findings of this study contradict the predictions of previous research. The theoretical procedure employed in this study indicated that the distorted capped octahedron

possesses a total energy that is 3.54 kcal/mol lower than that of the distorted pentagonal bipyramid.

The octamer ground state structure, as predicted by Aktürk and Sebetci (C_{2v}),[34] Cervantes-Salguero and Seminario (D_{2d}),[33] Diéguez *et al*.,[30] Köhler *et al*,[31] and Ma *et al*. (D_{2d}),[32] was a bidisphenoid (bicapped octahedron). The study commenced with the examination of cubic (O_h) and bidisphenoid (C_{2v}) structures, with a subsequent evaluation of multiplicities 21 and 25 for each. Following the optimization process, a transformation occurred in which the symmetries underwent a change from O_h to D_{4h} and from C_{2v} to C_1. The DKH2-B1B95/DZP+1*d*-DKH calculations demonstrated that the two structures with the lowest energies were from the C_1 point group, and the one with the highest multiplicity was 29.29 kcal/mol more stable (Fig. 1). It is evident that the symmetry predicted by the present study deviates from those symmetries that were previously determined.

Researchers have identified a bicapped pentagonal bipyramid (C_{2v})[32-34] or a tricapped trigonal prism (D_{3h})[30,31] as the most stable isomers of Fe_9. Consequently, an investigation was conducted into these two structures, with multiplicities of 19 and 27 being taken into consideration. The DKH2-B1B95/DZP+1*d*-DKH theoretical model predicted that the bicapped pentagonal bipyramid (C_s, M = 27) is 18.09 kcal/mol more stable than the tricapped trigonal prism (C_{2v}, M = 27). This occurrence signifies the inaugural documented instance of C_s symmetry for the bicapped pentagonal bipyramid of Fe_9.

In accordance with the findings of Ma *et al*. (C_{2v}),[32] Cervantes-Salguero and Seminario (C_{3v}),[33] and Aktürk and Sebetci (C_1),[34] the lowest energy structure of Fe_{10} is the tri-capped pentagonal bipyramid. This outcome is not consistent with the predictions of Dieguez *et al*.[30] and Köhler *et al*.,[31] who proposed a bicapped square

antiprism. In light of this uncertainty, an investigation was conducted into structures exhibiting D_{4d} and D_{2h} symmetries, in addition to the tri-capped pentagonal bipyramid. For each case, multiplicities of 29, 31, and 33 were evaluated. The two lowest-energy structures, in ascending order, were identified as the tri-capped pentagonal bipyramid (C_1), with M = 33 and 31, respectively. The second structure was found to be 5.46 kcal/mol less stable (Fig. 1).

DFT calculations cited in this work[30-32,34] verified that the ground state structure of Fe_{11} is a tetra-capped pentagonal bipyramid. In addition to this structure, which was initially classified as belonging to the C_{2v} point group, our investigation encompassed two other structures from our article on rhodium clusters.[42] One of these structures exhibited C_1 symmetry, while the other displayed C_{2v} symmetry. Multiplicities 31, 33, and 35 were considered in this study. Subsequent to optimization, the three tetra-capped pentagonal bipyramids underwent a relaxation process, resulting in a C_1 symmetry configuration. In contrast, the remaining structures retained their original symmetry. This symmetry is analogous to that obtained by Aktürk and Sebetci,[34] yet it differs from the C_{2v} symmetry identified by Ma *et al*.[32] for the ground state of Fe_{11}. DKH2-B1B95/DZP+1*d*-DKH calculations predicted a tetra-capped pentagonal bipyramid (M = 35) as the lowest energy structure (Fig. 1).

According to the findings of previous DFT studies,[30-32,34] the ground state of Fe_{12} is a penta-capped pentagonal bipyramid. However, a consensus has yet to be reached regarding the point group to which the cluster belongs: C_s[34] or C_{5v}.[32] Employing multiplicities 33, 35, 37, and 39, in conjunction with the penta-capped pentagonal bipyramid (C_{5v}) and double cube (D_{4h}) structures, a search was conducted for the structure with the lowest energy. Following the optimization process, a transformation from C_{5v} symmetry to C_1 was observed, resulting in the identification of

the penta-capped pentagonal bipyramid with M = 39 as the structure exhibiting the lowest energy, with a stability that is 11.30 kcal/mol higher than that of the corresponding structure with M = 37 (refer to Fig. 1 for visual representation).

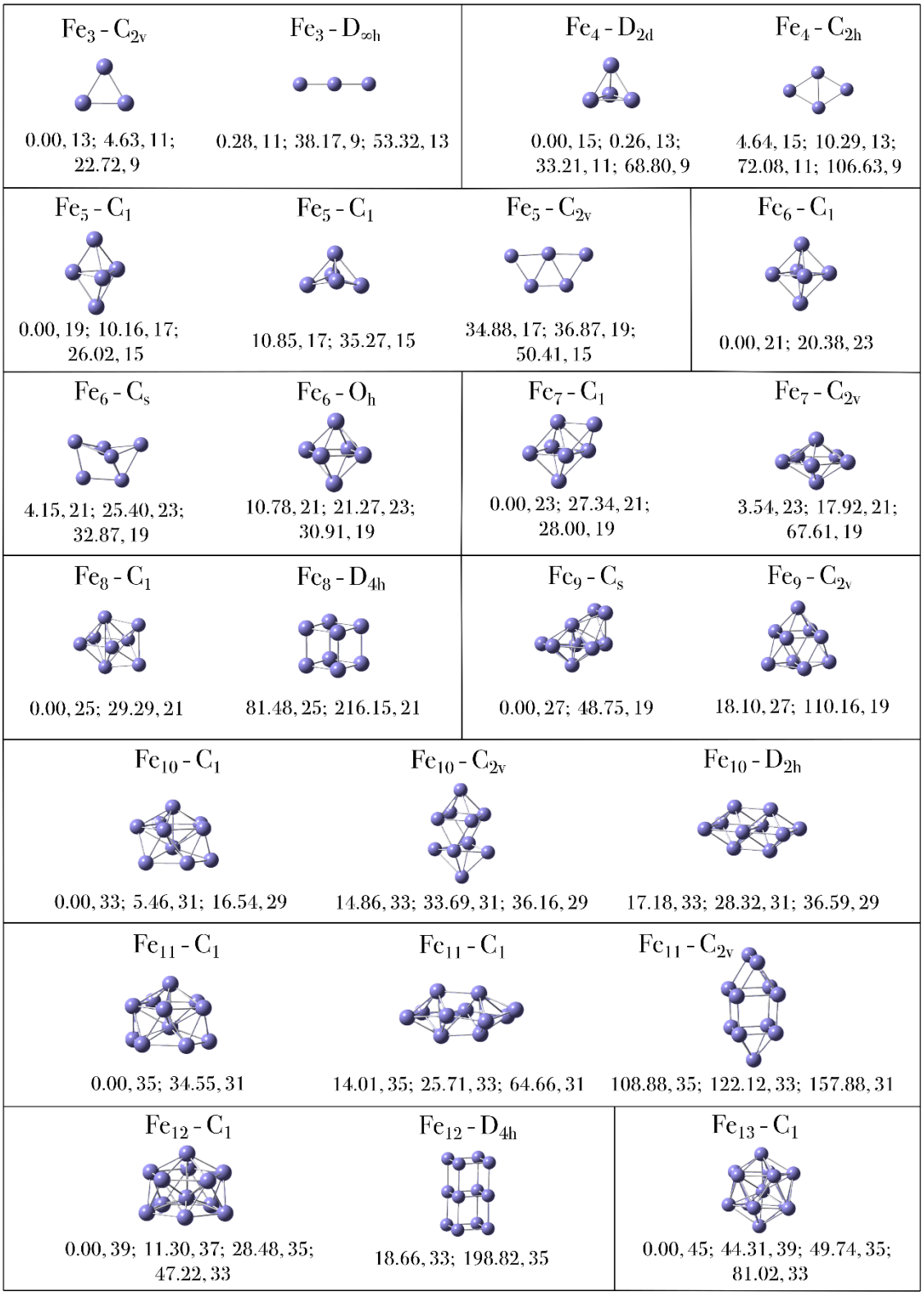


Fig. 1. DKH2-B1B95/DZP+1*d*-DKH optimized structures of the neutral Fe_n ($3 \leq n \leq 13$) clusters. Each pair of numbers bellow the structure corresponds to relative energy (in kcal/mol) and multiplicity of an isomer, while each semicolon separates information about two isomers.

It is imperative to ascertain the precise geometric structure of Fe_{13}, as it functions as a template for the formation of larger clusters. The potential modes of symmetry include icosahedral, hexagonal, cuboctahedral, and decahedral.[55] Previous theoretical studies have reached a consensus regarding the most stable configuration of Fe_{13}, which is determined to be a distorted icosahedron.[30-32,34] However, the symmetries identified (C_1[34] and D_{2h},[32]) are incompatible. Accordingly, the investigation was initiated with icosahedral (I_h) structures exhibiting multiplicities of 33, 35, 39, and 45, which were subsequently subjected to a process of optimization. Consequently, the total energies of the clusters (C_1 symmetry) exhibited an upward trend as the multiplicity value decreased, with a notable difference of 44.31 kcal/mol observed between the two most stable isomers (Fig. 1).

An analysis revealed that the Jahn-Teller effect was responsible for the distortions of the symmetric ground-state structures utilized as initial starting points for the optimization process of Fe_4, Fe_5, Fe_7, and Fe_{11} clusters. The distortions manifested in order to remove the degeneracy of the partially occupied HOMO.

The properties presented in the following **Sections** were computed based on the lowest energy structure of each iron cluster.

3.2. Bond Length

As illustrated in Table 2, the average bond lengths (R_{ave}) of the lowest energy structures of the iron clusters obtained with DKH2-B1B95/DZP+1*d*-DKH are presented. For the purpose of comparison, the results of non-relativistic BLYP/6-31G** and relativistic BLYP/SDD-ECP calculations are also included. The results of this study demonstrate an oscillation between Fe_2 and Fe_9, characterized by an even-odd pattern, wherein clusters with odd-numbered values exhibit higher R_{ave} values compared to their nearest neighbors. An oscillation of the average BLYP/SDD-ECP bond lengths is also

observed from Fe_5 to Fe_{10}; however, in this case, the even-numbered clusters dominate. The theoretical models demonstrate an increase in R_{ave} between Fe_{11} and Fe_{13}. A substantial degree of agreement is observed between the results obtained in this study and those derived through the BLYP/SDD-ECP procedure. However, a deterioration in the degree of agreement is evident when a comparison is made with BLYP/6-31G**. It is important to reiterate that the SDD-ECP basis set provides a description of the valence electrons of each iron atom, while the 6-31G** basis set encompasses all electrons. These findings suggest that relativistic corrections and basis sets have different effects on iron cluster bond lengths.

3.3. Stability

With the exception of Fe_3 at the DKH2B1B95/DZP+1*d*-DKH level, the three theoretical procedures demonstrate an increase in binding energies per atom (*BE*/n) from

Table 2. The average bond lengths (R_{ave}) and the binding energies per atom (*BE*/n) for the ground state iron clusters.

Cluster	Symmetry	R_{ave} (Å)		*BE*/n (eV)	
	(this work)	This work[a]	Literature[b]	This work[a]	Literature[b]
Fe_2	($D_{\infty h}$)	1.96	2.02 / 2.03	0.58	0.76 / 0.43
Fe_3	(C_{2v})	2.40	2.28 / 2.26	0.44	1.12 / 1.23
Fe_4	(D_{2h})	2.36	2.38 / 2.29	0.75	1.43 / 1.75
Fe_5	(C_1)	2.48	2.39 / 2.30	1.21	1.70 / 2.15
Fe_6	(C_1)	2.46	2.46 / 2.37	1.46	1.93 / 2.44
Fe_7	(C_1)	2.51	2.44 / 2.35	1.49	2.05 / 2.62
Fe_8	(C_1)	2.40	2.45 / 2.35	1.58	2.10 / 2.70
Fe_9	(C_s)	2.45	2.44 / 2.35	1.64	2.13 / 2.79
Fe_{10}	(C_1)	2.49	2.46 / 2.37	1.74	2.17 / 2.87
Fe_{11}	(C_1)	2.49	2.48 / 2.39	1.81	2.21 / 2.92
Fe_{12}	(C_1)	2.52	2.50 / 2.41	1.89	2.25 / 2.97
Fe_{13}	(C_1)	2.54	2.52 / 2.40	2.05	2.29 / 3.06

[a]DKH2-B1B95/DZP+1*d*-DKH calculations. [b]From Ref. [34]. The first and second values are the relativistic BLYP/SDD-ECP and non-relativistic BLYP/6-31G** calculations, respectively.

Fe_2 to Fe_{13} (see Table 2). This trend, which has also been documented by Diéguez *et al*.,[30] Köhler *et al*.,[31] Ma *et al*.[32] and Cervantes-Salguero and Seminario,[33] suggests that the geometric structures of neutral iron clusters become more stable as their size increases. Furthermore, it is predicted that the theoretical binding energies per atom should approach that of bulk iron (4.28 eV) for larger iron clusters. As the cluster size increases, the atoms acquire a higher coordination number, meaning that there are more chemical bonds. The increase in a cluster's coordination number is accompanied by increases in the binding energy per atom and the bond lengths between nearest-neighbor atoms. Conversely, the bond order—which measures the amount of charge along each chemical bond—decreases.[25] The average bond lengths and binding energies per atom (DKH2B1B95/DZP+1*d*-DKH) for the iron clusters shown in Table 2 are in complete agreement with these trends. It is noteworthy that the binding energies obtained in Ref. [33] is approximately equal to the values computed with the theoretical BLYP/SDD-ECP approximation,[34] while those found in Refs. [30-32] are larger. As demonstrated in Table 2, the magnitudes of the corresponding binding energies decrease in the following order: The initial two are BLYP/6-31G** and BLYP/SDD-ECP, while the latter is DKH2B1B95/DZP+1*d*-DKH. It is noteworthy that the order of bond lengths was precisely inverse, as longer bond lengths are linked to reduced binding energies per atom. As previously mentioned, the experimental *BE*/n value of the iron dimer is [0.57±0.05] eV. As illustrated in Table 2, only our value falls within the experimental uncertainty bars. In contrast, the BLYP/6-31G** and BLYP/SDD-ECP results are overestimated and underestimated, respectively. This phenomenon elucidates the reason behind the systematically elevated *BE*/n values observed in the other clusters in comparison to our own. The DKH2B1B95/DZP+1*d*-DKH model is expected to provide

reliable results because it considers both the scalar relativistic correction and a basis set that describes all electrons.

As illustrated in Fig. 2, there is an evident oscillatory pattern in the dissociation energies from Fe_2 to Fe_6 and from Fe_7 to Fe_{12}. In the first and second intervals, respectively, maxima occur for clusters containing odd and even numbers of atoms. Two peak points are evident on the D_e curve: one at Fe_5 and one at Fe_{13}. This finding suggests that these two clusters exhibit elevated thermodynamic stability. It is noteworthy that n = 6 does not correspond to one of the maxima on the curve; however, the dissociation energy of Fe_6 (2.659 eV) is the fourth highest. The dissociation energy curve obtained by

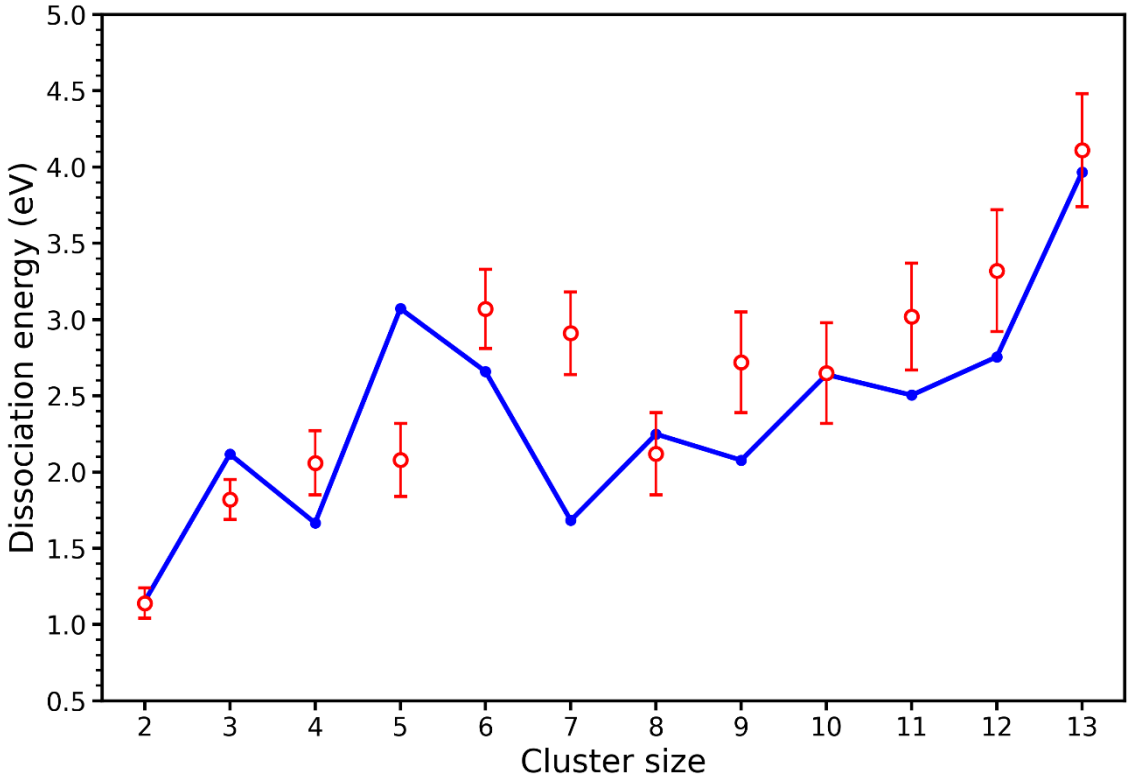


Fig. 2. DKH2-B1B95/DZP+1*d*-DKH (filled blue circles) and experimental[9] (open red circles) dissociation energies for Fe_n ($2 \le n \le 13$) clusters.

Cervantes-Salguero and Seminario[33] shows increasing behavior from Fe_2 to Fe_6, followed by a decrease to Fe_9, then a slight increase to Fe_{10}. These researchers hypothesize that Fe_6 is the most stable structure up to Fe_{10}. Given the inherent uncertainties associated with the collision-induced dissociation measurements conducted by Lian *et al.*,[9] the results of our study appear to be consistent with theirs. Indeed, the aforementioned authors estimated these dissociation energies using an indirect method. They measured the dissociation energies of the cationic clusters Fe_n^+ and determined the corresponding values for the neutral clusters using the ionization potentials of neutral clusters measured by Yang and Knickelbein[10] and Rohlfing *et al.*[51] That is to say,

$D(Fe_n) = D^{exp}(Fe_n^+) + IP^{exp}(Fe_n) - IP^{exp}(Fe_{n-1})$. This is undoubtedly one of the factors contributing to the observed discrepancy between the experimental and theoretical dissociation energies depicted in Fig. 2 for Fe_5 and Fe_7. In fact, the experimental dissociation energy of an iron cluster represents an average over a set of isomers exhibiting varied geometries and/or multiplicities. In contrast, the DKH2-B1B95/DZP+1*d*-DKH result is associated exclusively with the cluster's lowest-energy structure. This is yet another factor that exacerbates the lack of agreement between the experimental and theoretical results. As illustrated in Fig. 1, isomers exhibiting total energy differences of 5 kcal/mol or less are exclusively observed for clusters ranging from Fe_3 to Fe_7. This finding suggests that these isomers make a substantial contribution to the measured dissociation energy value. As demonstrated in Fig, 2, the poorest agreement between theoretical and experimental results was observed for Fe_5 and Fe_7, which are clusters belonging to the range from n = 3 to n = 7. According to the work of Lian *et al.*,[9] the similarity observed in the dissociation energies of Fe_n and Fe_n^+ indicates that electronic effects do not predominate as the primary factors determining

the relative stabilities of iron clusters. This observation suggests that geometric structure is the determining factor. With this in mind, we can predict the geometric shapes of the stable 5-, 6-, and 13-atom clusters shown in Fig. 2: the trigonal bipyramid, octahedron, and icosahedron, respectively. The optimized geometric structures obtained using the B1B95/DZP+1*d*-DKH theoretical model are in full agreement with these predictions.

The second-order difference in total energies (Δ^2E) is a quantitative metric that assesses the stability of a cluster of n atoms in comparison to clusters of n − 1 and n + 1 atoms. The peaks of this curve correspond to what are known as magic numbers. As illustrated in Fig. 3, the values of Δ^2E for Fe_n clusters ($2 \leq n \leq 12$) are presented as a

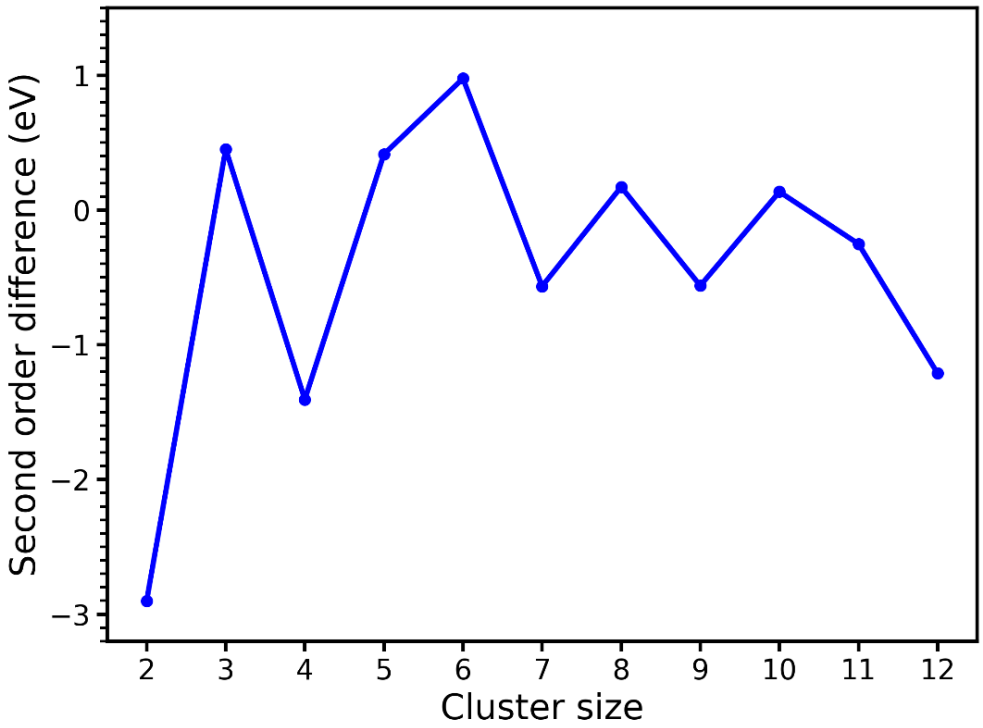


Fig. 3. DKH2-B1B95/DZP+1*d*-DKH second-order differences in total energies for Fe_n ($2 \leq n \leq 12$) clusters.

function of cluster size. A review of the interval reveals the presence of even-odd oscillations. Maxima are observed at n = 3, 6, 8, and 10. With the exception of n = 6, these maxima correspond to those observed in D_e's curve. The maximum at n = 6 in Fig.

3 suggests that six is the predicted magic number within the specified interval. This outcome aligns with one of the magic numbers identified by Ma *et al*.[32] The findings of our study are consistent with the results reported by Diéguez *et al*.,[30] Köhler *et al*.,[31] and Cervantes-Salguero and Seminario[33] who observed a decline in the Δ^2E plots at n = 7. Conversely, Aktürk and Sebetci[34] reported a slight peak with the BLYP/6-31G** theoretical model. The following magic numbers were determined for iron clusters using time-of-flight mass spectra: n = 7, 13, 15, 19, and 23.[17] However, the peak at n = 7 was less clear for post-ionized iron clusters. Instead of a peak at n = 7, we obtained one at n = 6. This discrepancy is likely attributable to the ionization of the clusters in the experiments, as they were conducted at elevated temperatures. However, the calculations were performed at 0 K. Zhang *et al*.[56] attribute this discrepancy to thermal effects.

3.4. Electronic properties

The HOMO-LUMO energy gap (E_g) of a cluster is associated with its chemical activity. The magnitude of E_g, whether large or small, is indicative of low or high chemical activity, respectively. The results in Table 3, presented in descending order, indicate that the most reactive clusters are Fe_2, Fe_9, and Fe_{12}, while the least reactive clusters are Fe_3, Fe_6, and Fe_5. This finding indicates that Fe_6 can be utilized as a unit cell in the construction of larger clusters, while Fe_9 and Fe_{12} are effective in catalytic reactions. As illustrated in Fig. 2, the results for D_e align with those for E_g, as the maxima of this curve are observed at n = 3 and 5, and the minima are at n = 2 and 9. As illustrated in Fig. 3, the Δ^2E results are consistent with those obtained for E_g, given that the maxima are observed at n = 3 and 6, and the minima at n = 2, 9, and 12. In summary, elevated values of E_g contribute to the stabilization of Fe_3, Fe_5, and Fe_6 clusters.

Conversely, low values of E_g render Fe_2, Fe_9, and Fe_{12} clusters less stable and, consequently, more reactive.

The vertical ionization potentials (*VIP*s) of Fe_n ($2 \leq n \leq 13$) are enumerated in Table 3. The determination of the lowest-energy isomer for each cation was achieved through the utilization of the geometry of the corresponding neutral cluster, in conjunction with various multiplicities. Given that each iron atom possesses a total of 26 electrons, singly ionized clusters with an even or odd number of atoms are known to accept only even multiplicities. In this study, the *VIP* concept is associated with the energy required to remove an electron from an iron cluster. As illustrated in Table 3, the *VIP*s of the iron clusters obtained with DKH2-B1B95/DZP+1*d*-DKH are presented. The precision of these values was evaluated by comparing them with experimental data.[10,51]

Table 3. The HOMO-LUMO energy gaps (E_g) and vertical ionization potentials (*VIP*) for the ground state iron clusters.

Cluster	E_g (eV)	*VIP* (eV)		
	This work[a]	This work[a]	Literature[b]	Experimental[c]
Fe_2	1.21	6.04	5.81	6.30±0.01[d]
Fe_3	2.46	6.04	5.15	6.45±0.05[d]
Fe_4	1.41	5.85	5.43	6.40±0.10[d]
Fe_5	2.21	6.24	5.42	5.95±0.05[d]
Fe_6	2.25	5.09	5.79	5.96±0.05
Fe_7	1.76	4.96	5.41	5.76±0.05
Fe_8	1.67	5.40	5.20	5.48±0.05
Fe_9	1.23	4.47	4.66	5.50±0.05
Fe_{10}	1.27	4.74	4.26	5.41±0.05
Fe_{11}	1.32	4.72	–	5.45 ±0.05
Fe_{12}	1.23	5.04	–	5.52±0.05
Fe_{13}	1.25	5.14	–	5.61 ±0.05

[a]DKH2-BLYP/DZP+1*d*-DKH calculations. [b]From Ref. [33]. The results were derived from non-relativistic OPBE/TZV calculations. [c]From Ref. [51]. [d]From Ref. [10].

The behavior of the *VIP*s obtained in this study resembles that of the experimental data: the highest values are concentrated between Fe_2 and Fe_5, followed by a gradual decrease

from Fe_5 to Fe_{11}, then an increase from Fe_{11} to Fe_{13}. With the exception of a few cases, our results from Fe_2 to Fe_{10} are more aligned with the experimental data[10,51] than the *VIP*s calculated with the OPBE/TZV procedure.[33] Overall, there is a high degree of agreement between the DKH2-B1B95/DZP+1*d*-DKH values and the experimental values. This contributes to the credibility of the lower-energy geometric structures determined for the Fe_n and Fe_n^+ clusters in this article.

3.5. Polarizabilities

The electron cloud of an iron cluster undergoes a distortion when exposed to an external electric field. This phenomenon is referred to as dipole polarizability. The mean dipole polarizabilities ($\bar{\alpha}$), mean dipole polarizabilities per atom ($\bar{\alpha}$ /n), and polarizability anisotropies ($\Delta\alpha$) of Fe_n ($2 \leq n \leq 13$) clusters were computed at the DKH2-BLYP/ADZP-DKH level, and the results are included in Table 4. It is important to note that the self-consistent field procedure for the polarizability calculations of some iron clusters did not converge with the B1B95 functional. Consequently, a change of functional was necessary. The BLYP functional was selected because it had previously been employed successfully to determine the polarizabilities of rhodium[42] and cobalt[43] clusters and because, as will be demonstrated below, this change of functional does not affect the predictions derived from the polarizability results, since they are consistent with those based on HOMO-LUMO energy gaps, dissociation energies, and second-order differences in total energies.

The increasing number of electrons from Fe_2 to Fe_{13} directly results in the systematic growth of $\bar{\alpha}$. An analysis of the $\bar{\alpha}$ /n results is imperative because it provides information about the iron cluster structures. The relationship between E_g and $\bar{\alpha}$ /n is generally verifiable; that is to say, the smaller the E_g value, the less stable the cluster, and the larger the $\bar{\alpha}$ /n value. Nevertheless, given the dependence of the

magnitude of $\bar{\alpha}$ /n on the geometric shape of the cluster, its final value is the sum of the two contributions. In certain instances, geometry emerges as the predominant factor, while in others, E_g assumes a similar role. In summary, the stability of an iron cluster is contingent upon its high E_g value and geometric symmetry. In light of the aforementioned facts, the mean dipole polarizabilities per atom presented in Table 4 are now comprehensible. An increase in E_g is observed when transitioning from Fe_2 to Fe_3, as illustrated in Table 3. In this particular instance, the concomitant growth of $\bar{\alpha}$ /n is attributable to the fact that the larger cluster is affiliated with a higher point group (see Fig. 1). The magnitude of $\bar{\alpha}$ /n increases from Fe_3 to Fe_4 for two reasons. It can be posited that the decrease in the E_g value is concomitant with the increased symmetry of Fe_4 (D_{2h}) in comparison to Fe_3 (C_{2v}). As the transition progresses from Fe_4 to Fe_5, a decrease in the symmetry of the cluster from C_{2v}

Table 4. Static mean dipole polarizabilities ($\bar{\alpha}$), mean dipole polarizabilities per atom ($\bar{\alpha}$ /n), and polarizability anisotropies ($\Delta\alpha$) for the ground state iron clusters. All values are in a.u.

Cluster	DKH2-BLYP/ADZP-DKH		
	$\bar{\alpha}$	$\bar{\alpha}$ /n	$\Delta\alpha$
Fe_2 ($D_{\infty h}$)	86.58	43.29	41.63
Fe_3 (C_{2v})	145.81	48.60	78.20
Fe_4 (D_{2h})	196.40	49.10	64.47
Fe_5 (C_1)	223.31	44.66	48.36
Fe_6 (C_1)	240.68	40.11	9.29
Fe_7 (C_1)	276.70	39.53	83.28
Fe_8 (C_1)	300.14	37.52	78.33
Fe_9 (C_s)	338.00	37.55	88.26
Fe_{10} (C_1)	379.95	38.00	136.98
Fe_{11} (C_1)	404.50	36.77	104.10
Fe_{12} (C_1)	429.16	35.76	70.96
Fe_{13} (C_1)	453.03	34.85	20.35

to C_1 is observed, concomitant with an increase in E_g, leading to a corresponding decrease in $\bar{\alpha}$ /n. As the parameter E_g increases, the value of $\bar{\alpha}$ /n decreases from Fe_5 to

Fe_6. As illustrated in Fig. 1, a reduction in symmetry is evident from Fe_6 to Fe_7 and from Fe_7 to Fe_8. In such instances, geometry emerges as the predominant factor, leading to a steady decline in $\bar{\alpha}$ /n. As demonstrated in Fig. 1, Fe_9 (C_s) exhibits a lower E_g value in comparison to Fe_8 (C_1). This observation serves to substantiate the higher $\bar{\alpha}$ /n value observed in Fe_9 (C_s). It has been demonstrated that, commencing at n = 10, all clusters exhibit C_1 symmetry. The behavior of E_g is the inverse of that of $\bar{\alpha}$ /n from Fe_{10} to Fe_{11} and from Fe_{12} to Fe_{13}.

The magnitude of polarizability anisotropy ($\Delta\alpha$), which is defined as the degree to which the system's charge distribution exhibits anisotropy, is a crucial factor in understanding the system's behavior. As the charge distribution approaches spherical symmetry, the value of the quantity decreases. As demonstrated in Table 4, Fe_6 and Fe_{10} were the clusters with the smallest and largest $\Delta\alpha$ values, respectively. This finding indicates that the geometric structure of Fe_6, as illustrated in Fig. 1, underwent a slight distortion from the O_h symmetry, which displays a spherical charge distribution. The small polarizability anisotropy of Fe_{13} is similarly justified, with the exception of the reference point group, which is I_h instead of O_h. The transition from a two-dimensional to a three-dimensional structure is accompanied by a decrease in the $\Delta\alpha$ value from Fe_3 to Fe_4. The charge distribution of a triangular bipyramid exhibits a greater degree of proximity to spherical symmetry in comparison to that of a triangular pyramid. This observation provides a rationale for the $\Delta\alpha$ values observed in clusters with n = 4 and 5. The reduction followed by an increase in polarizability anisotropy through the sequence $Fe_7 \rightarrow Fe_8 \rightarrow Fe_9$ can be explained by analyzing the geometric modifications undergone by these clusters (Fig. 1). The significant increase in $\Delta\alpha$ from Fe_9 to Fe_{10} indicates that the charge distribution of the latter cluster has become more diffuse. A similar finding was detected in the study of cobalt clusters performed at the same theoretical level.[43]

From Fe_{10} onwards, there is a gradual decrease in polarizability anisotropies as the clusters approach icosahedral symmetry. A thorough examination of the curves illustrated in Figs. 2 and 3, in conjunction with the findings outlined in Table 4, unveils a discernible correlation between the stability and charge distribution of a cluster. Specifically, clusters Fe_5, Fe_6, and Fe_{13} demonstrate the highest D_e and/or Δ^2E values and the lowest $\Delta\alpha$ values. This finding suggests that clusters exhibiting charge distributions that approximate spherical symmetry are among the most stable. A study of cobalt clusters[43] employing the same theoretical procedure as that of the present work demonstrates that this observation is also applicable.

3.6. Spin magnetic moment

The parallel alignment of electrons in iron, cobalt, and nickel clusters gives rise to the high-spin magnetic moments observed in these systems.[2-5] The total magnetic moments per atom (μ_T/atom) for the clusters Fe_n and Fe_n^+ ($2 \leq n \leq 13$) obtained with DKH2-B1BP95/DZP+1*d*-DKH, as well as the theoretical values reported by Diéguez *et al*.,[30] Köhler *et al*.,[31] Ma *et al*.,[32] and Aktürk and Sebetci[34] for the neutral clusters, are included in Table 5. The present study found experimental data for simply ionized iron clusters in the existing literature.[19,20] These data were included in Table 5 to assess the precision of the present study's results.

For neutral clusters, our results demonstrate an odd-even oscillation of spin magnetic moments from n = 2 to n = 6, with maxima occurring in clusters with an odd number of atoms. Among all clusters, Fe_3 exhibits the highest spin magnetic moment. As illustrated in Fig. 1, the disparity in relative energy between the two isomers of Fe_3, an isosceles triangle with M = 13 and a linear one with M = 11, is a mere 0.28 kcal/mol. Given the necessity of these two isomers in the spin magnetic moment measurement, the μ_T/atom value of this cluster, as presented in Table 5, should undergo reduction. The

calculation of the weighted average of the spin magnetic moments of both isomers is essential for obtaining an accurate result. A similar analysis can be applied to the two spin isomers (M = 15 and M = 13) of Fe_4. Subsequent to Fe_6, the μ_T/atom values undergo a decline until they reach the nadir of the curve at Fe_9. An odd-even oscillation is observed again from Fe_9 to Fe_{12}. The maxima occur for even n values. Finally, from Fe_{12} to Fe_{13}, there is a slight increase in the spin magnetic moment. The spin magnetic moments per atom of the neutral iron clusters are all higher than the experimental bulk value of 2.2 μ_B.[19]

Table 5. Spin magnetic moments per atom (μ_T/atom, μ_B) for Fe_n and Fe_n^+ clusters in the ground state.

	Neutral				Cation	
n	This work[a]	Ref. [32][b]	Ref. [34][c]	Ref. [30,31][d]	This work[a]	Exp.[e]
2	3.00	-	3.00 / 4.00	3.00	3.50	3.25±0.50
3	4.00	3.33	3.33	2.67	3.00	2.40±0.40
4	3.50	3.50	3.50	3.00	3.25	2.50±0.40
5	3.60	3.26	3.20	3.20 / 2.80	3.40	2.60±0.40
6	3.33	3.33	3.33	3.33	3.50	3.13±0.40
7	3.14	3.14	3.14	3.14	3.28	3.18±0.40
8	3.00	3.00	3.00	3.00	3.38	3.20±0.40
9	2.89	2.89	2.89	2.89	3.00	2.78±0.40
10	3.20	3.10	3.00	2.80	3.30	3.33±0.19
11	3.09	3.09	3.09	2.73	3.36	3.30±0.42
12	3.17	3.00	3.17	2.67	3.25	3.41±0.50
13	3.38	3.38	3.38 / 2.62	2.62	2.69	2.44±0.38

[a]Results obtained from DKH2-B1B95/DZP+1*d*-DKH calculations. [b]Results obtained from BLYP/DNP calculations. [c]Whenever they differ, the BLYP/SDD and BLYP/6-31G** calculations are presented as the first and the second values, respectively. [d]Whenever they differ, the LSDA/LCNAO[30] and DFTB/LCSTO[31] calculations are presented as the first and the second values, respectively. [e]From Refs. [19,20].

Despite the absence of consensus on the ground-state geometric structures, a range of calculations[30-34] based on density functional theory (DFT), employing different functionals and/or basis sets, have yielded similar μ_T/atom values for Fe_6 to Fe_9 (see Table 5). However, the magnetic spin moments per atom of the other clusters

exhibit variation. In light of the aforementioned uncertainties, a calculation was conducted to determine the spin magnetic moments per atom of Fe_n^+. Given the existence of experimental data for these clusters, they will facilitate the evaluation of the reliability of the DKH2-B1B95/DZP+1*d*-DKH theoretical procedure in determining this property.

The spin magnetic moments per atom for the cations differ from those obtained for the neutral clusters and range from 2.69 μ_B (for Fe_{13}^+) to 3.50 μ_B (for Fe_2^+ and Fe_6^+). With the exception of Fe_3^+ and Fe_4^+, for which the DKH2-B1B95/DZP+1*d*-DKH results are marginally overestimated, all other μ_T/atom values are within the ranges covered by the experimental measurements' uncertainties. This outcome lends further credence to the efficacy of the selected theoretical model. The extant literature contains physical arguments that elucidate the origin of the abrupt drop in μ_T/atom from Fe_{12}^+ to Fe_{13}^+. In certain instances, density functional theory (DFT) modeling[30,57] predicts a decrease in the magnetic spin moment of neutral Fe_{13} due to antiferromagnetic spin coupling of the central atom with other atoms. As indicated by our findings, more recent theoretical research[58,59] has also demonstrated an increase in μ_T/atom from Fe_{12} to Fe_{13}, attributable to enhanced contributions from the 4*s* orbital to the spin magnetic moment. It is imperative to acknowledge that Köhler *et al*. exclusively considered the spin isomer with multiplicity 35 for Fe_{13}.[31] However, our calculations demonstrated that the total energy of this isomer is 49.74 kcal/mol higher than that of the most spin-stable isomer (M = 45) (see Fig. 1).

4. Conclusions

The theoretical procedure DKH2-B1B95/DZP+1*d*-DKH selected in this work (see Table 1) was the same as that used in the study of cobalt clusters.[43] This approach

was chosen to contribute to the elucidation of controversial points concerning the geometric structures and multiplicities of small iron clusters. The distinguishing feature of this model, which sets it apart from all previous models utilized in the investigation of small iron clusters, is its capacity to account for all electrons in the system and the scalar relativistic correction simultaneously. The observed discrepancies between the property results obtained in this study and those reported by Diéguez *et al*. (LSDA/ LCNAO),[30] Köhler *et al*. (DFTB/LCSTO),[31] Ma *et al*. (BLYP/DNP),[32] Cervantes-Salguero and Seminario (OPBE/TZV),[33] and Aktürk and Sebetci (BLYP/6-31G**)[34] are primarily attributable to the use of non-relativistic DFT calculations with a non-relativistic basis set by these authors. Aktürk and Sebetci (BLYP/SDD-ECP)[34] were the only researchers to perform a relativistic calculation; however, their approach utilized a basis set that exclusively encompassed the valence electrons. With respect to the ground-state structures of the iron clusters, it has been observed that the absence of constraints during the optimization process, in conjunction with the utilization of the DKH2-B1B95/DZP+1*d*-DKH approximation, has given rise to a geometric structure for Fe_7 and symmetries for Fe_5, Fe_6, Fe_8, Fe_9, and Fe_{12} that have not been previously documented in the extant literature. It is important to reiterate that, for each iron cluster that was studied, a significant number of spin multiplicities were examined to ascertain the ground state. This exhaustive search led to the determination of previously unreported spin magnetic moments per atom for Fe_3, Fe_5, and Fe_{10}. The DKH2-B1B95/DZP+1*d*-DKH procedure enabled the determination of spin magnetic moments per atom for Fe_n^+ clusters that rank among the most accurate published to date. To the best of our knowledge, this is the first time calculations of mean dipole polarizabilities and polarizability anisotropies have been performed to aid in identifying the most stable and most reactive iron clusters.

The geometric structures of the most stable isomers identified in this study do not always align with the predictions in the referenced literature.[30-32] In the case of the heptamer, this constitutes the first instance in which a distorted capped octahedron, rather than a pentagonal bipyramid, has been documented as the ground-state geometric structure. In instances where they do coincide, disparities may emerge with respect to the point group to which they belong.[30-34] To obtain more realistic electronic structures, no restrictions were imposed on the optimization process. Consequently, a relaxation of the initial symmetry was observed for all structures, with most reducing to the C_1 point group. Conversely, certain authors have employed a methodology that preserves symmetry during the optimization process, thereby yielding structures classified as belonging to higher-order point groups.

An odd-even oscillation is evident in the average DKH2-B1B95/DZP+1*d*-DKH bond lengths from Fe_2 to Fe_9, while an increase is observed from Fe_{11} to Fe_{13}. The favorable alignment between our results and those obtained using an alternative relativistic approximation (BLYP/SDD-ECP)[34] lends credibility to the ground state geometric structures we predicted.

The DKH2-B1B95/DZP+1*d*-DKH binding energies per atom demonstrate an increase with cluster size, with the exception of Fe_3. For Fe_2, the result obtained in this study is the only one that falls within the experimental error margin. In contrast, the results computed using alternative theoretical procedures [30-34] are consistently higher than the experimental data. This observation elucidates the reason why previously documented binding energies per atom[30-34] for the other clusters are higher than those observed in this study.

The DKH2-B1B95/DZP+1*d*-DKH dissociation energy curve exhibits odd-even oscillations. These oscillations result in two maximal points that stand out from the

others, indicating the high thermodynamic stabilities of Fe_5 and Fe_{13}. A close examination of the results reveals a strong correlation with the experimental data. Additionally, the graph of second-order differences in total energies calculated in this study exhibited odd-even oscillations. The predicted numerical value of n, which corresponds to the magic number, is determined to be 6. With the exception of one point, the maxima predicted by the D_e and Δ^2E curves coincide. The energy gaps between the HOMO and LUMO levels indicate that Fe_9 and Fe_{12} are among the most reactive clusters, while Fe_6 is among the least reactive. The predictions derived from the HOMO-LUMO and Δ^2E results exhibit a high degree of consistency with one another. As with the HOMO-LUMO energy gap and dissociation energies, the DKH2-B1B95/DZP+1*d*-DKH vertical ionization potentials suggest that Fe_3 and Fe_5 are among the most stable clusters. The strong correlation between the experimental and DKH2-B1B95/DZP+1*d*-DKH vertical ionization potentials supports the reliability of the geometric structures of the lowest-energy neutral and cationic isomers predicted in this study.

As anticipated, the mean dipole polarizability exhibited a gradual increase in conjunction with the number of atoms within the cluster. The present study confirmed the relationship between the mean dipole polarizability per atom and the HOMO-LUMO energy gap. Specifically, an increase in E_g from the n-1 cluster to the n cluster was observed to be concomitant with a decrease in $\bar{\alpha}$/n, and vice versa. The lowest polarizability anisotropy value was obtained for Fe_6, followed by Fe_{13}. This finding suggests that the first cluster exhibited a lower degree of distortion of the O_h symmetry compared to the second cluster, which demonstrated a higher degree of distortion of the I_h symmetry. It is noteworthy that both point groups exhibit a spherical charge distribution. The findings of this study suggest that clusters exhibiting charge

distributions that approximate spherical symmetry are among the most stable. The maximum $\Delta\alpha$ value, which occurred for Fe_{10}, suggests that this cluster has the most diffuse charge distribution. It is noteworthy that this is the inaugural instance in which polarizabilities have been calculated for iron clusters. The enhancement in the comprehension of iron cluster electronic structures, as evidenced by these results, suggests that future studies will likely employ this powerful tool.

The spin magnetic moments per atom of neutral iron clusters exhibit odd-even oscillations from n = 2 to n = 6 and from n = 9 to n = 12. A decline in values is observed between n = 6 and n = 9, followed by an increase from n = 12 to n = 13. The largest and smallest values were identified for n = 3 and n = 9, respectively. It is evident that all of these values exceed the measured bulk value of 2.2 μ_B. The magnitudes of the spin magnetic moments per atom found in this study and in the works of other authors are not always consistent. For cations, the spin magnetic moments differ from those of neutral clusters and range from 2.69 to 3.50 μ_B. With the exception of Fe_3^+ and Fe_4^+, whose DKH2-B1B95/DZP+1*d*-DKH results are slightly overestimated, the rest are within the uncertainty bars of the experimental data. The accuracy achieved for the μ_T/atom values of the cations classifies our results as being among the most remarkable documented in the extant literature. This finding provides compelling justification for the credibility of the ground-state geometric and electronic structures determined for the iron clusters examined in this study.

The theoretical procedure DKH2-BLYP/DZP+1*d*-DKH has once again demonstrated its efficacy in calculating the diverse properties of transition metal clusters. Additionally, it has contributed to the elucidation of controversial points regarding the geometric and electronic structures of small iron clusters.

Acknowledgments

We would like to acknowledge the financial support provided by the following Brazilian agencies: Fundação de Amparo à Pesquisa e Inovação do Espírito Santo (FAPES) and Conselho Nacional de Desenvolvimento Científico e Tecnológico (CNPq).

References

[1] Zhao J, Huang X, Jin P and Chen Z 2015 *Coord. Chem. Rev.* **289-290** 315.

[2] Zhi-Da C, Tao L and Jing Z 2010 *Chin. Phys. B* **19** 057101.

[3] Pastor G M, Dorantes-Davila J and Benneman K H 1989 *Phys. Rev. B* **40** 7642–7654.

[4] Fujima N and Yamaguchi T 1989 *J. Phys. Soc. Jpn.* **58** 3290–3297.

[5] Dunlap B I 1990 *Phys. Rev. A* **41** 5691–5694.

[6] Billas I M L, Châtelain A and de Heer W A 1997 *J. Magn. Magn. Mater*. **168** 64.

[7] Cox D M, Trevor D J, Whetten R L, Rohlfing E A and Kaldor A 1985 *Phys. Rev. B* **32** 7290.

[8] Billas I M L, Châtelain A and de Heer W A 1994 *Science* **265** 1682.

[9] Lian L, Su C-X and Armentrout P B 1992 *J. Chem. Phys*. **97** 4072.

[10] Yang S and Knickelbein M B 1990 *J. Chem. Phys.* **93** 1533.

[11] Griffin J B and Armentrout P B 1997 *J. Chem. Phys*. **107** 5345.

[12] Andersson M, Persson J L and Rosén A 1996 *J. Phys. Chem*. **100** 12222.

[13] Schnabel P, Weil K G and Irion M P 1992 *Angew. Chem. Int. Ed. Engl.* **31** 636.

[14] Pellarin M, Baguenard B, Vialle J L, Lerme´ J, Broyer M, Miller J and Perez A (1994) *Chem. Phys. Lett.* **217** 349.

[15] Parks E K, Weiller B H, Bechthold P S, Hoffman W F, Nieman G C, Pobo L G and Riley S J 1988 *J. Chem. Phys*. **88** 1622.

[16] Parks E K, Winter B J, Klots T D and Riley S J 1992 *J. Chem. Phys*. **96** 8267.

[17] Sakurai M, Watanabe K, Sumiyama K and Suzuki K 1999 *J. Chem. Phys*. **111** 235.

[18] Wang L-S, Cheng H-S and Fan J 1995 *J. Chem. Phys*. **102** 9480.

[19] Niemeyer M, Hirsch K, Zamudio-Bayer V, Langenberg A, Vogel M, Kossick M, Ebrecht C, Egashira K, Terasaki A, Moller T, Issendorff B v and Lau J T 2012 *Phys. Rev. Lett*. **108** 057201.

[20] Langenberg A, Hirsch K, Lawicki A, Zamudio-Bayer V, Niemeyer M, Chmiela P, Langbehn B, Terasaki A, Issendorff B v and Lau J T 2014 *Phys. Rev*. B **90** 184420.

[21] Knickelbein M B 2002 *Chem. Phys. Lett*. **353** 221.

[22] Xu X, Yin S, Moro R, Liang A, Bowlan J and de Heer W A 2011 *Phys. Rev. Lett*. **107** 057203.

[23] Harvey J N (2004) *Struct. Bond* **112** 151-184.

[24] Chen J L, Wang C S, Jackson K A and Pederson M R 1991 *Phys. Rev. B* **44** 6558.

[25] Castro M, Jamorski C and Salahub D R 1997 *Chem. Phys. Lett*. **271** 133.

[26] Ballone P and Jones R O 1995 *Chem. Phys. Lett*. **233** 632.

[27] Oda T, Pasquarello A and Car R 1998 *Phys. Rev. Lett*. **80** 3622.

[28] Andriotis A N and Menon M 1998 *Phys. Rev. B* **57** 10 069.

[29] Freeman A J, Li C and Wu R Q 1991 *Science and Technology of Nanostructured Magnetic Materials*, Vol. 259 of *NATO Advanced Study Institute, Series B: Physics*, edited by Hadjipanayis G C and Prinz G A (Plenum, New York), p. 1.

[30] Diéguez O, Alemany M M G, Rey C, Ordejón P and Gallego L J 2001 *Phys. Rev. B* **63** 205407.

[31] Köhler C, Seifert G and Frauenheim T 2005 *Chem. Phys*. **309** 23–31.

[32] Ma Q-M, Xie Z, Wang J, Liu Y and Li Y-Ch 2007 *Solid State Commun*. **142** 114–119.

[33] Cervantes-Salguero K and Seminario J M 2012 *J. Mol. Model*. **18** 4043–4052.

[34] Aktürk A and Sebetcib A 2016 *AIP Adv***. 6** 055103.

[35] Perdew J and Schmidt K 2001 *AIP Conf. Proc*. **577** 1.

[36] Douglas M and Kroll N M 1974 *Ann. Phys*. **82** 89.

[37] Hess B A 1986 *Phys. Rev. A* **33** 3742.

[38] Jorge F E, Ferreira I B, Soprani D D and Gomes T 2016 *J. Braz. Chem. Soc.* **27** 127.

[39] Jorge F E, de Macedo L G M 2016 *Chin. Phys. B* **25** 123102.

[40] Jorge F E and Santos A S 2018 *J. Braz. Chem. Soc*. **29** 838.

[41] Jorge F E and Venancio J R C 2018 *Chin. Phys. B* **27** 063102.

[42] De Oliveira A Z and Jorge F E 2020 *Comput. Theor. Chem*. **1177** 112765.

[43] Ceolin G A, Sampaio G R C, Campos C T and Jorge F E 2025 *Braz. J. Phys*. **55** 262.

[44] Frisch M J, Trucks G W, Schlegel H B, *et al*. 2009 Gaussian 09, Revision A.02, (Gaussian Inc., Wallingford, CT).

[45] Jorge F E, Canal Neto A, Camiletti G G and Machado S F 2009 *J. Chem. Phys*. **130** 064108.

[46] Camiletti G G, Canal Neto A, Jorge F E and Machado S F 2009 *J. Mol. Struct: THEOCHEM* **910** 122.

[47] Montano P A and Shenoy G K 1980 *Solid. State Commun*. **35** 53.

[48] Purdum H, Montano P A, Shenoy G K and Morrison T 1982 *Phys. Rev. B* **25** 4412.

[49] Moskovits M and DiLella D P 1980 *J. Chem. Phys*. **73** 4917.

[50] Andrade S G, Goncalves L C S and Jorge F E 2008 *J. Mol. Struct. THEOCHEM* **864** 20.

[51] Rohlfing E A, Cox D M, Kaldor A and Johnson K H 1984 *J. Chern. Phys*. **81** 3846.

[52] Du J, Sun X and Wang H 2008 *Int. J. Quantum Chem*. **108** 1505.

[53] Chrétien S and Salahub D R 2002 *Phys. Rev. B* **66** 155425.

[54] Micklitz H, Pasternak M and Sanchez J P 1985 *Solid State Commun*. **55** 667.

[55] Akola J, Häkkinen H and Manninen M 1998 *Phys. Rev. B* **58** 3601.

[56] Zhang W H, Liu L, Zhuang J, Li Y F 2000 *Phys. Rev. B* **62** 8276.

[57] Bobadova-Parvanova P, Jackson K A, Srinivas S and Horoi M 2002 *Phys. Rev. B* **66** 195402.

[58] Wu M, Kandalam A K, Gutsev G L and Jena P 2012 *Phys. Rev. B* **86** 174410.

[59] Rollmann G, Entel P and Sahoo S 2006 Comput. Mater. Sci. **35** 275.